NUMERICAL SIMULATIONS AROUND WING CONTROL SURFACES

Guillaume Fillola
AIRBUS, Toulouse, Fr

Marie-Claire Le Pape
ONERA, Châtillon, Fr

Marc Montagnac
CERFACS, Toulouse, Fr

Keywords: *Aileron, Spoiler, Chimera Mesh, Patched Grid, Wall Law*

ABSTRACT

A study of wing control surface effectiveness was carried out using numerical simulations with the advanced Reynolds Averaged Navier-Stokes solver ***elsA.*** *Non-coincident meshing techniques were used as to make the mesh generation process more flexible. The first application attempts to predict an aileron effectiveness using the patched grid meshing technique combined with a mesh deformation tool in order to operate the aileron deflection. The second one deals with spoiler deployment and involves the Chimera technique, which allows separating the spoiler meshing from the wing meshing and so avoiding a complete mesh re-generation for each spoiler deflection.*

NOMENCLATURE

α	Angle of attack
β	Sideslip angle
δa	Aileron deflection angle
δs	Spoiler deflection angle
M_0	Free stream mach number
Re	Reynolds number
q/E	Aero-elastic coefficient (q is the dynamic pressure and E the Young's modulus)
CL	Lift coefficient
CD	Drag coefficient
Cl	Rolling moment coefficient
Cm_c	Hinge moment coefficient
φ	Twist angle
x/c	Adimensioned coordinate x by the local chord
y_{ch}	Adimensioned coordinate y by half span, $=(y-y_{root})/b$
ch_z	Local load in z direction

1 INTRODUCTION

The correct prediction of handling qualities and hinge moments induced by the deployment of wing control surfaces (spoilers and ailerons) is a crucial point in the general aircraft sizing process with a strong impact on the final aircraft weight. The complexity of the aerodynamic flows around deployed control surfaces and the importance of the flight envelope to be covered made difficult the use of CFD in the elaboration of Aerodynamic Data. Until now, only very time-consuming and costly wind tunnel tests and not very accurate semi-empirical methods were used.

For a long time, CFD has been intensively used at Airbus for shape design and optimization. As configurations are moderately complex and studies focused on slight geometrical variations, an efficient coincident structured mesh generation suite has been set up around HEXA© mesher.

Thanks to the recent CFD progress in meshing techniques, convergence acceleration and calculation performance, more and more numerical simulations are involved in Aerodynamic Data generation. However, the classic coincident structured grid approach does not seem suitable for complex configurations such as deployed ailerons and spoilers.

Today, the following meshing techniques appear to us as the most promising for control surfaces configurations:

- **The *Patched-Grid* technique,** which allows meshing independently on each side of shared boundaries between two blocks, is thus more appropriate to build independent wing section grids.
- **The *Chimera* technique** is almost the same technique as the Patched Grid method but is further enriched by the overlapping grid capability. Its principle is to mesh independently different bodies and then to take into account interactions between the different components by interpolations.
- **The *Wall Law* technique** consists in applying the "linear-logarithmic" law on the first cell, the size of which can be much larger than $y^+=1$. Performance is then improved during calculation without downgrading the solution accuracy. Moreover, it facilitates interpolation issues for Chimera technique.

This paper first presents a brief summary of the flow solver ***elsA***, as well as the particular techniques to be used. Following is a discussion around two numerical simulations, with comparison to experimental results. Aileron effectiveness results using the Patched Grid technique will be presented first, followed by spoiler effectiveness results using the Chimera technique.

2 NUMERICAL METHODS

2.1 *elsA* solver

With the objective of federating all national research teams and taking advantage of older functionalities implemented in separate CFD codes, ONERA has been developing a new generation solver called ***elsA*** since 1996, in co-operation with CERFACS since 2000. It has been designed according to an Object Oriented design method and it is mainly coded with C++ language, even though the most CPU-expensive loops are coded with Fortran language for better numerical efficiency. This innovative approach leads to more upgradeable and inter-operable aerodynamic functions, and thus contributes to a better integration of different development [1]. Some applications made in Airbus France with the ***elsA*** solver are described in [2].

The main features and numerical functions of ***elsA*** are listed below:

- cell centered code dealing with structured meshes.
- classical central scheme for Euler model (centered flux with scalar dissipation)
- viscous flux computed from cell-centered evaluations of velocity and temperature gradients, with possible correction values at interfaces.
- classical algebraic and transport equations turbulence models (all of them following Boussinesq's assumption).
- backward-Euler time integration associated with the LU implicit method.
- Wall Law treatment possibility for wall boundary conditions [3].

We describe below the specific techniques used in this study for aircraft applications.

2.2 *Patched Grid* technique

Complex configurations are decomposed in many structured meshes. These blocks are connected to each other with shared interfaces that impose constraints on the grid generation. Indeed, a local mesh refinement in one of the blocks spreads through the entire computational domain with classical coincident structured grids.

The *Patched-Grid* technique allows meshing two blocks independently on each side of their shared boundaries. A local mesh refinement has then a lesser impact on the other blocks. Thus the computer memory required and CPU time are reduced since the number of grid points decreases.

The most important characteristic of this technique is to provide the conservation property of the numerical scheme as shown in [4] and [5]. This paper uses the approach described in [6]. Further details, complements or other methods related to this technique can be found for example in [7], [8], [9] and [10].

A bi-dimensional overview of the patched grid technique is shown in Figure 1.

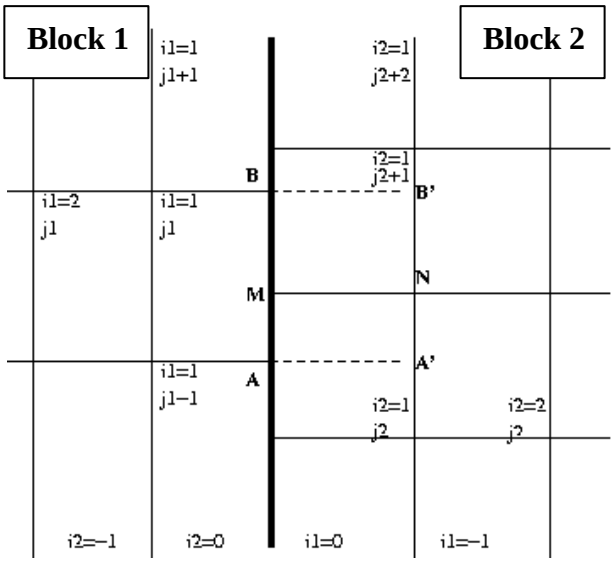

Figure 1 : Two blocks with a shared patched grid interface.

The indices (i,j) refer to the location of cells in both blocks and the border surface is located at the index ½. For comprehensive purposes, it is assumed that the border surface is plane that is to say there is neither overlapping nor gaps between cells that are next to the surface border. The principle of the patched grid is explained with the example of the cell (i1,j1) of block 1. The numerical flux through the interface AB can be written:

$$F^1_{AB} = F^1_{1/2,\,j1} = aF^1_{AM}(W_{i1,\,j1}, W_{i2,\,j2}) + (1-a)F^1_{BM}(W_{i1,\,j1}, W_{i2,\,j2+1}) \quad (1)$$

with $a = \frac{|AM|}{|AB|}$ and W represents the conservative state vector or any other fields and α is the intersection area computed from the two border interfaces of the cells (i1,j1) and (i2,j2). The intersection surface of these two interfaces is obtained with the intersection polygon given by a Sutherland-Hodgman polygon-clipping algorithm [11].

This treatment of spatial fluxes enables to maintain the global conservation along the patched grid border surface. Indeed, the above operations are applied on each block independently and hence $F^1_{AM} = F^2_{AM}$ for planar border surfaces. If the border surface is curved, then this technique is said quasi-conservative since F^1_{AM} and F^2_{AM} might slightly differ according to the point projection process.

The ghost cells are filled thanks to an α-weighted interpolation process of the state vector in order to keep the efficiency of implicit time-integration algorithms.

2.3 *Chimera* technique

The ***Chimera method*** is based on an overset grid technique [12]. The principle is to generate independent meshes around different body elements, and to solve the global flow by using interpolation technique in the CFD solver. More precisely, on the one hand the mesh areas overlapped by bodies are not computed by the solver and body influence comes from a cell crown around each body; on the other hand, domain influence goes through outflow boundaries. This technique allows almost independ body meshing; meshes must only sufficiently overlap to allow interpolations. As for the independent bodies, refined meshes make this constraint respected. However, when bodies are next to each other and because of blanking, areas near junctions are not discretized. In order to by-pass this difficulty, the solution - used in the present work - is to generate a mesh leaning on the body of the other mesh.

In the ***elsA*** software, the interpolation is piecewise linear by tetrahedron, each cell being divided into 24 tetrahedrons. Bodies are modeled by a great number of parallelepipeds. Interpolation cell search becomes efficient by using a preconditioned Cartesian grid and other acceleration techniques to find the interpolation tetrahedron [13]. In order to reduce overlapping constraints and to avoid some points from becoming orphan, extrapolation from neighbouring cells is allowed; the numerical scheme is also degenerated on overlapping boundaries and around bodies, thus

interpolation crown and boundaries have a width of one cell [14].

3 AIRCRAFT APPLICATIONS

3.1 Prediction of aileron effectiveness using the *Patched Grid* technique

Aircraft wings are equipped with ailerons that have several functions in terms of handling qualities. They are usually activated to create a rolling moment with a dissymmetrical deflection; but they are also deflected in a symmetrical way in order to modify punctually the aircraft lift (in high lift configuration for example). Aerodynamically, an aileron pulls up or down the aft part of a small wing section, modifying so the local load. As a result, the global lift and/or the rolling moment change.

This first application aims thus at predicting the variation of global aerodynamic coefficients due to an aileron deflection in a transonic flow field. The studied configuration is a half wing-body equipped with an outboard aileron separated from the wing by two lateral gaps; it is the model used in the HiReTT European project [15]. The surface definition of the wing corresponds to $32.5.10^6$ Reynolds number and q/E=0.4395 wind tunnel conditions. Some calculations on the same configuration have already been done in Airbus in the HiReTT framework [16] with a different meshing approach.

3.1.1 Grid generation process

With a traditional coincident mesh, the aileron deflection would lead to shear cells confined in the gap area. One way of overcoming this problem consists in meshing independently the aileron wing section by placing two vertical patched grid plans in the middle of each gap (Figure 2). In this way, the aileron deflection will only modify the area between the two patched grid plans not degrading the cell skewness. The mesh topology is a typical wing-body mesh of 6.500.000 nodes, with a CH grid around the fuselage, and a CH grid around the wing completed by a pivot on the wing tip.

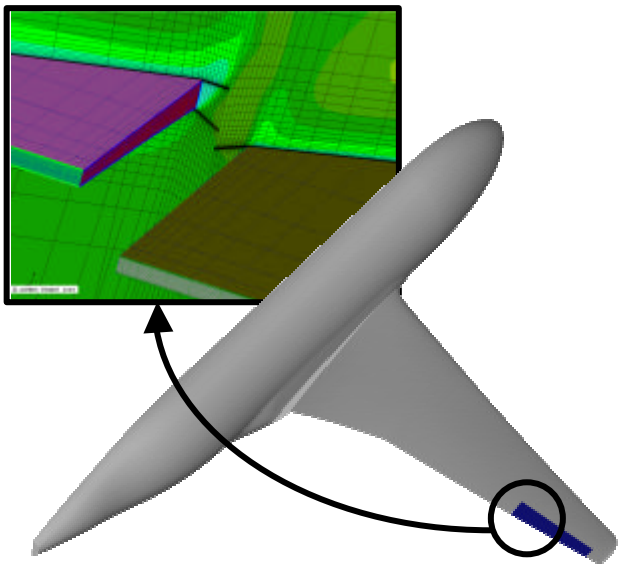

Figure 2 : HiReTT wing-body with a d a=3° deflected aileron – inner gap overview

In order to speed up the mesh generation process, a mesh deformation procedure, called RAiD (Rudder and Aileron Deflection) dedicated to control surfaces deflection has been developed. It is composed of two independent programs.

The first one generates a surface field (dx,dy,dz) simulating the aileron deflection. It consists in calculating the control surface movement with respect to a hinge axis and then to operate a smooth joining of this area to the wing box, preserving the continuity in position and tangency. The second one, called VOLDEF, propagates this deformation in the mesh volume using an analytical method developed in Airbus [17]. It is based on the distinction between two kinds of surfaces:

- *Modified surfaces* G_m: which contain the surface field
- *Damping surfaces* G_a: which are not deformed

The deformation applied to a point M is thus given by the following formula:

$$\vec{d}(M) = h \cdot \frac{\int_{P \in \Gamma m} \frac{\vec{d}(P)}{d(M,P)^a} d\Gamma}{\int_{P \in \Gamma m} \frac{1}{d(M,P)^a} d\Gamma}, \ \alpha > 2 \qquad (2)$$

η is a damping function. This parameter has a value of 1 near a modified surface and tends toward 0 near a damping surface.

$$h = e^{-k\left(\frac{dm}{da}\right)^b} \qquad (3)$$

with $dm = \min_{P\in\Gamma m}(d(M,P))$ and $da = \min_{P\in\Gamma a}(d(M,P))$

This procedure allows obtaining a new mesh with an aileron deflected in less than 3 hours on a workstation and, thus, a wide range of deflected configurations can be easily inspected.

Figure 3 depicts a bi-dimensional application of the RAiD procedure applied on a simple OAT15A profile.

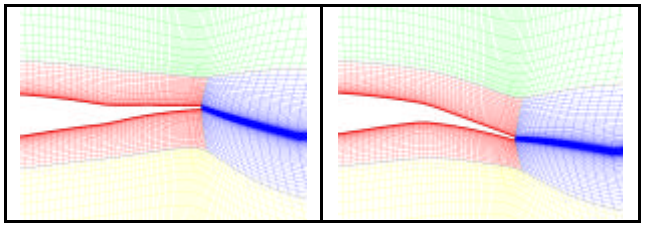

Figure 3 : aileron deflection by the mesh deformation procedure (left δa=-10°, right δa=+10°)

3.1.2 Discussion of results

On the basis of the clean configuration, three aileron settings (δa=-3°, 3°, 6°) are operated with the RAiD procedure. Turbulent calculations are then performed on each mesh, although we only have experimental results at δa=0° and 3°. The flow parameters are the following:

- M_0=0.85, α=1.5°
- Re_c=32.5 10^6, q/E=0.4395
- [SA] turbulent model in fully turbulent flow

Figure 4 presents results in terms of CL effectiveness (experimental CL is measured with balances). A nearly linear behavior appears at low deflections, δa=-3° and +3°, whereas an obvious non-linearity occurs at δa=6°. At δ=3°, the computed global lift on clean configuration approximately matches the experimental value. However, the increment of lift induced by the aileron deployment is not well simulated. Thus, although errors between calculation and experiment at both δa=0° and 3° are less than 4% on global CL, this error reaches more than 100% on ΔCL!

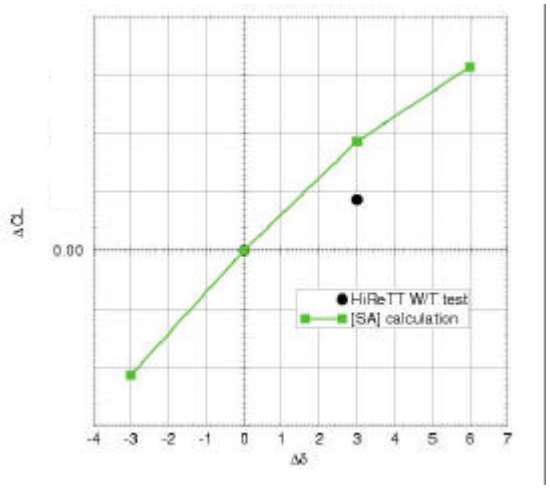

Figure 4: Aileron effectiveness, M_0=0.85, a =1.5°

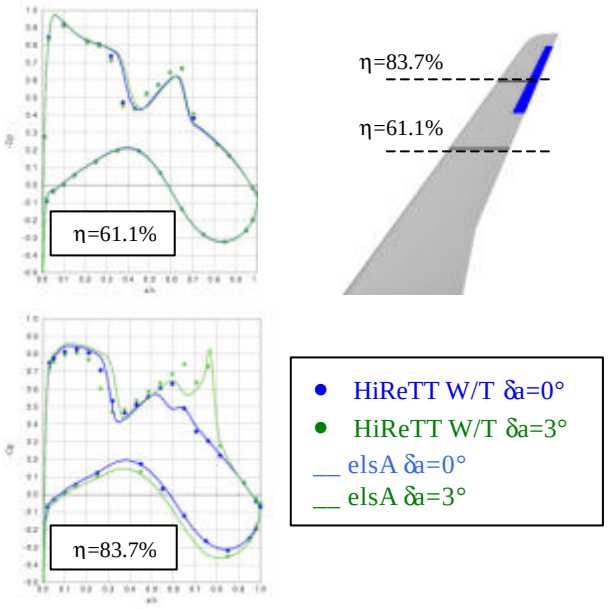

Figure 5 : Cp distribution for 2 deflected configurations, δa=0° and 3°, M_0=0.85, a =1.5°

On the Figure 5, Cp-distributions around two wing sections (one located on the middle of the wing, the other one at half span of the aileron) are represented, for two deflected configurations, δa=0° and 3°. (Unfortunately, three pressure probes, located on aileron lower surface, failed during the W/T test on the deflected configuration.) First of all, we observe that the structure of the flow is quite well

simulated on the clean configuration. Indeed, CFD predicts well the double shock topology and sets it roughly at the good location. The main aileron deployment effects are also well captured by the calculation: the lower surface pressure increases and a suction peek appears along the hinge line.

The shock location and the supersonic area level express the major discrepancy between calculation and experiment. We can see on Figure 6 that δa=3° calculation predicts a too-far-aft shock location, as well as an over-estimation of the supersonic plateau. Nevertheless, the comparison between non-deflected/deflected calculations highlights a consistent behaviour of the flow with a bi-dimensional approach (see [18]). On the contrary, in the experiment the shock moves forward and the supersonic plateau decreases making us thinking about an aero-elastic effect.

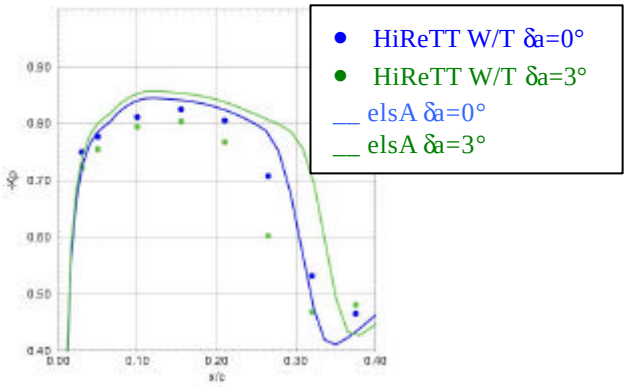

Figure 6 : Cp distribution on the aileron section, zoom on the supersonic area

In the HiReTT project framework, direct aero-elastic calculations have been done on this studied configuration, at the RWTH University [19]. It allows estimating the aerodynamic deformation only due to an aileron deflection. These results have been provided to us in term of twist angle and wing bending (Figure 7). They enlighten a slight reduction of the twist angle (φ_{max}~0.3°) in aileron sections (η=0.7 to 0.95). This is mainly due to the elevation of aft-load implying aileron sections to pitch down.

This deformation has been applied to our rigid deflected mesh using the VOLDEF procedure (Figure 8) and another ***elsA*** calculation has been carried out with the same flow parameters.

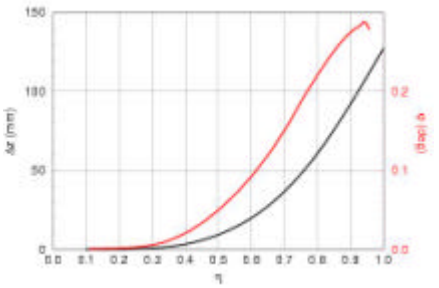

Figure 7 : Wing bending and twist angle due to a δa=3° aileron deflection.

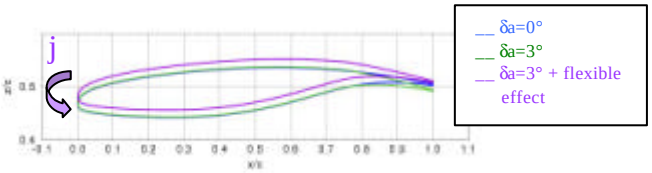

Figure 8 : Aero-elastic effect on the aileron section

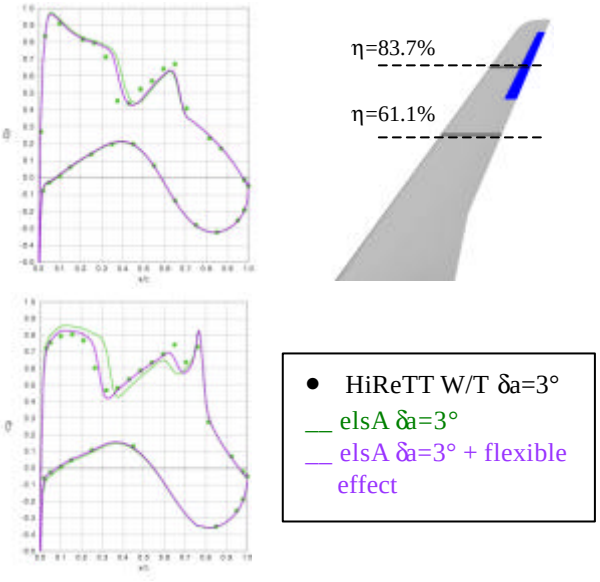

Figure 9 : Cp-distribution on the δa=3° configuration, flexible effect, M_0=0.85, α=1.5°

The reduction of the twist angle in aileron sections involves a reduction of the effective angle of attack. As the consequence the shock moves forward, the supersonic plateau decreases, and the calculated flow better matches to experimental values (Figure 9). This movement results in a slight decrease of the deflected configuration lift, and thus, a good

agreement is found in term of ΔCL ($\Delta CL_{flexible}/\Delta CL_{exp}$=90%, Figure 10).

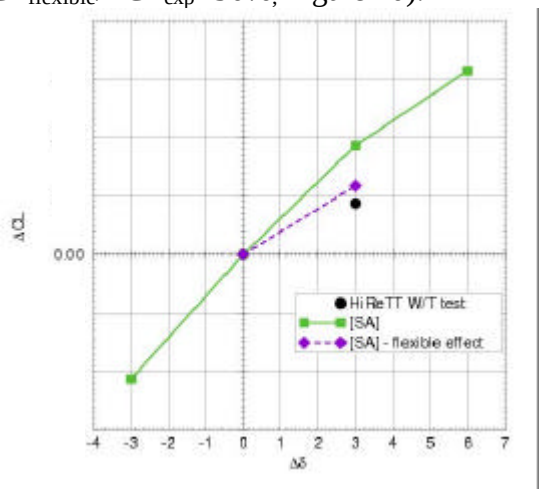

Figure 10 : Aileron effectiveness, flexibility effect, M_0=0.85, a =1.5°

3.2 Prediction of spoiler effectiveness using the *Chimera* technique

This second application intends to simulate the influence of spoiler deployment on global aerodynamic coefficients in a transonic flow field. A spoiler is a control device located in the middle of the upper wing, which produces flow separation when it is deflected. It causes therefore the lift to decrease and the drag to increase. When they are symmetrically deflected, spoilers are used as airbrakes and play a part in landing or during an emergency descent. With a dissymmetrical deflection, they intervene to accentuate aileron action and thus to create a high level of rolling moment

The studied configuration represents a typical AIRBUS wing body with external spoilers deployed. The wing shape corresponds to wind tunnel condition (5.10^6 Reynolds number) and was assumed as rigid when spoilers are deflected.

3.1.1 Grid generation process

The complex geometry of the studied configuration leads us to use the Chimera technique. Actually, one multi-block grid of 3.500.000 nodes is dedicated to the wing + body whereas another one of 500.000 nodes, totally independent, is dedicated to the spoilers and a wing portion (Figure 11). Thus, the meshing procedure is made simpler and a good mesh quality can be easily ensured.

Because the spoiler is joined to the wing, we have chosen to define a part of the wing both in the spoiler mesh and in the wing-body mesh, in order to avoid the presence of orphan points at the intersection between the wing and the spoiler. Then, the wing grid is holed at the spoiler location in order to take into account the spoiler presence.

This double discretization of the wing was causing interpolation problems in the original low Reynolds mesh because of the surface curvature. Actually, cells closed to one body can be located inside the second one. This problem is well known and Schwarz proposes a solution in [20] that should be soon integrated in ***elsA***. Waiting for this, we overcome the limitation by using wall law technique.

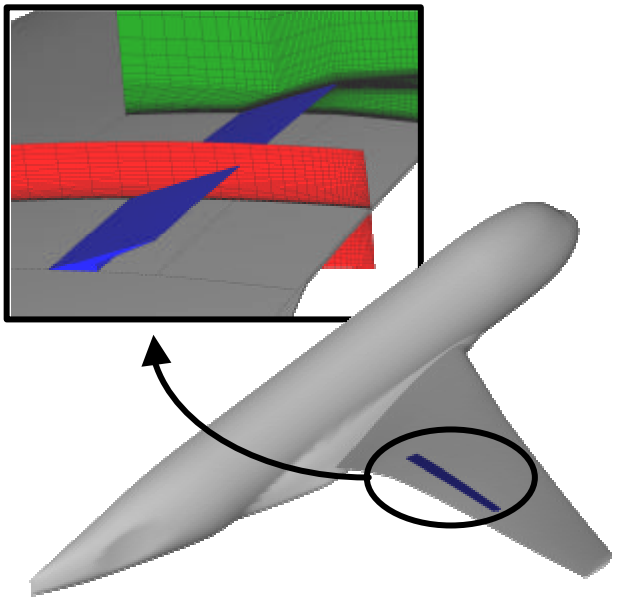

Figure 11 : Airbus wing-body with a ds=20° deflected spoiler

Another interesting feature of the Chimera technique is that the spoiler deflection will only affect the spoiler domain, and so a complete mesh re-generation is not necessary for every spoiler setting.

3.1.2 Discussion of results

To validate our calculations, we rely on experimental results coming from a wind tunnel

test campaign with few Cp measurements. The mock-up is a complete aircraft with pods, flap-trap-fairings, horizontal and vertical tail planes (H/VTP), and we will compare it to our calculations around a simple wing-body. These differences between the two configurations involve several aero dynamical discrepancies that we will describe below.

The HTP increases the CL_α slope because the local HTP angle of attack increases when α increases (despite a reduction due to wing downwash). The pods induce a negative ΔCL (almost constant with α), mainly due to a forward location of the shock. However, these impacts are the same on the clean wing and on the wing with a deployed spoiler; that is why we will only express our results in term of variation with respect to the clean wing characteristics.

The following calculation matrix has been carried out for three deflected configurations, δs=0°, 20° and 45°:

δs=0°, 20°, 45°		α						
		0	2.5	3.5	4.0	5.0	6.0	7.0
M	0.7	x	x			x	x	x
	0.85	x	x	x	x	x		

Table 12 : calculation matrix

Lift Effectiveness

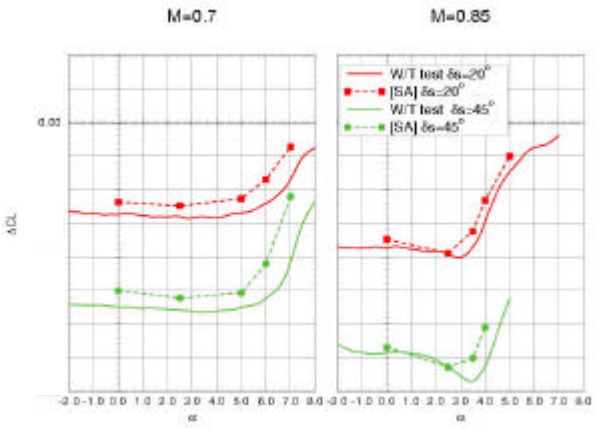

Figure 13 : CL spoiler effectiveness, *left* δs=20°, *right* δs=45°, M_0=0.7, 0.85 (line : experiment, symbols : calculations)

A good agreement between experiment and numerical calculations is found on $\Delta CL(\alpha)$ (Figure 13). This curve is characterized by two regimes. At low angles of attack, ΔCL is almost constant (this level is quite well simulated by CFD at M_0=0.85). At high angles of attack, a non-linearity appears, bringing about a drop of ΔCL. This phenomenon occurs because, for a given α, the wing with a deflected spoiler stays linear whereas first non-linearity appears on clean wing (Figure 14).

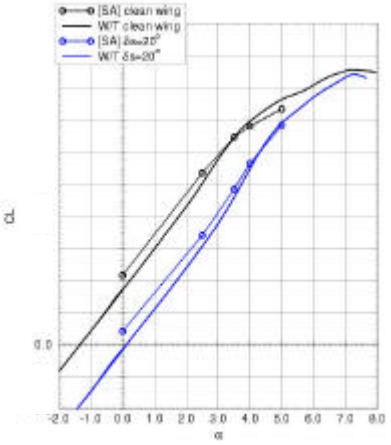

Figure 14 : CL(α) δs=0°,45°, M_0=0.85

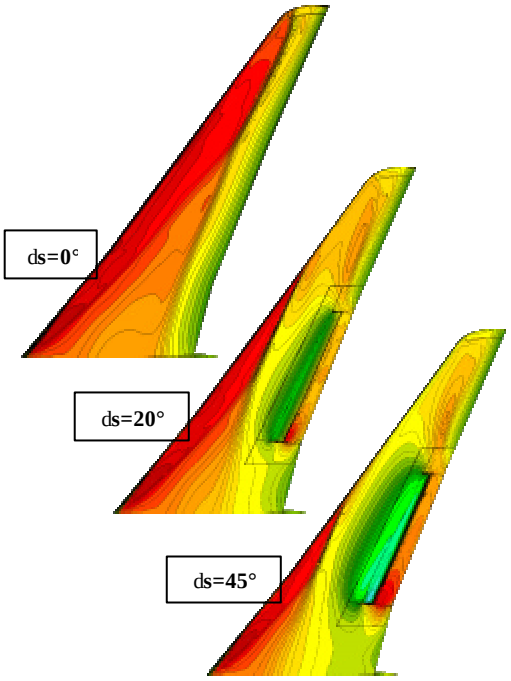

Figure 15 : -Cp distribution on δs=0°, 20°, 45° deflected wing, M_0=0.85, α=2.5°

On Figure 15 a visualization of the flow through –Cp distribution, around three deflected wings is given. The spoiler deployment pushes forward the shock wave and thereby causes the loss of lift. On the spoiler upper surface the pressure increases with the spoiler deflection

whereas a strong acceleration appears on the inner spoiler lower surface. It creates high differences between the spoilers' hinge moments.

Spoiler Hinge Moment

Hinge moment coefficients on each spoiler are plotted on Figure 16. Because of the lower surfaces over-speed, the inner spoiler Cm_c is quite more negative than the other spoiler's ones.

At high angles of attack, a shock separation appears and encompasses the spoilers, beginning at the outer spoilers (Figure 17, the red surfaces show the separation area). This causes these spoilers Cm_c to increase until they become positive.

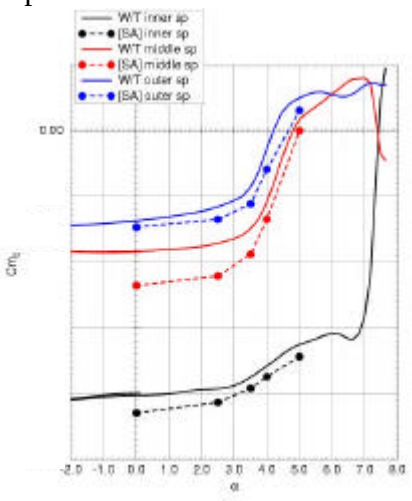

Figure 16 : Spoilers hinge moment (Cm_c), $\delta s=20°$, $M_0=0.85$ (line : experiment, symbols : calculations)

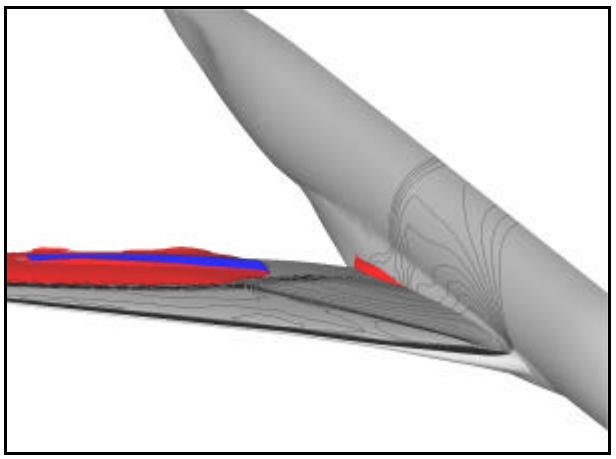

Figure 17 : visualization of separation area (in red) – spoiler in blue – $M_0=0.85$, $\alpha=5.0°$

Drag Effectiveness

Near field drag has also been investigated. Results in term of ΔCD are presented in Figure 18. The main effects of spoiler deflection are well captured by CFD: ΔCD decreases when α increases until becoming negative at high angles of attack (meaning that spoiler deployment reduces drag instead of increasing it).

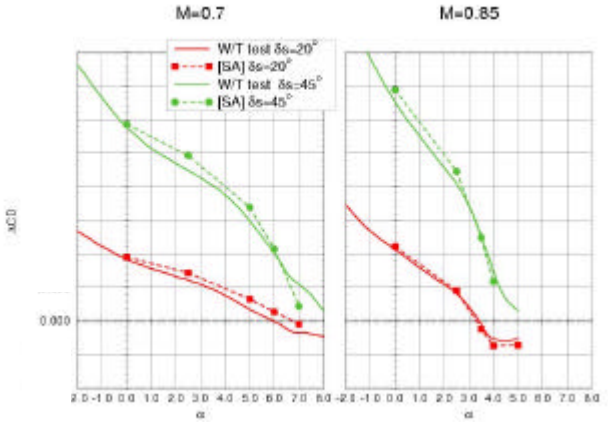

Figure 18 : CD spoiler effectiveness, $\delta s=20°$, $M_0=0.7$, 0.85 (line : experiment, symbols : calculations)

Rolling Moment Effectiveness

The rolling moment effectiveness analysis highlights a discrepancy between calculation and experiment that does not appear on the lift effectiveness curve. ΔCl is overestimated (in modulus, Figure 20) while ΔCL better matches experiment (Figure 13).

Taking advantage of the Chimera method flexibility, a new mesh representing a complete dissymmetrical aircraft with a spoiler deflected on the left wing, has been rapidly built. On Figure 19, the wings loads of this complete aircraft are compared to the half aircraft ones. The differences between the two wing loads highlight an interaction between the left and the right wing. Right wing inner load decreases while left wing inner load increases; as a result, the rolling moment decreases and compares fairly to experimental values (Figure 20). The $\Delta CL(\alpha)$ curve is quite the same as the half aircraft one because of a compensation phenomenon between right and left wing's lift.

Another result of the complete aircraft computation is the creation of a sideslip field of

about 1° at the fin location (see Figure 21). Airbus Cl_β data modeling indicates that this impact would cause a positive Cl responsible of an additional ΔCl around 0.01.

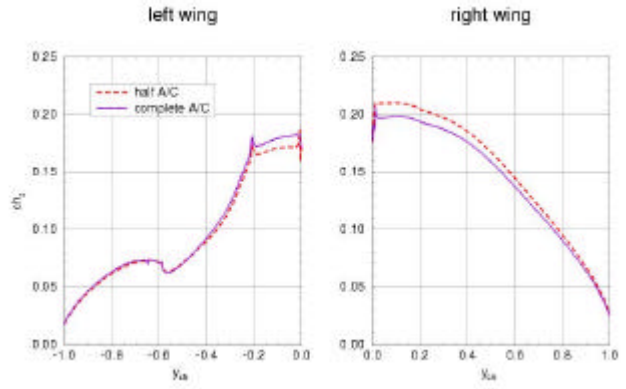

Figure 19 : Computed wing load - interaction left wing/ right wing – M_0=0.85, α **=2.5°**

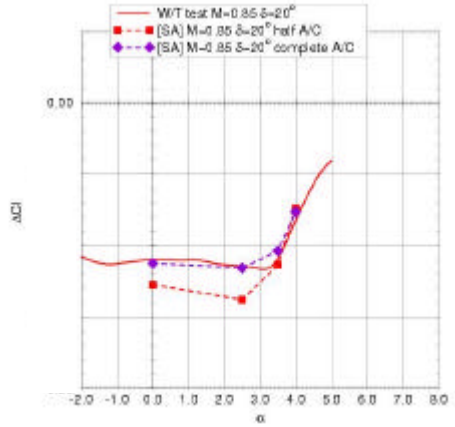

Figure 20 : Cl spoiler effectiveness – δs**=20° - M_0=0.85 (line : experiment, symbols : calculations)**

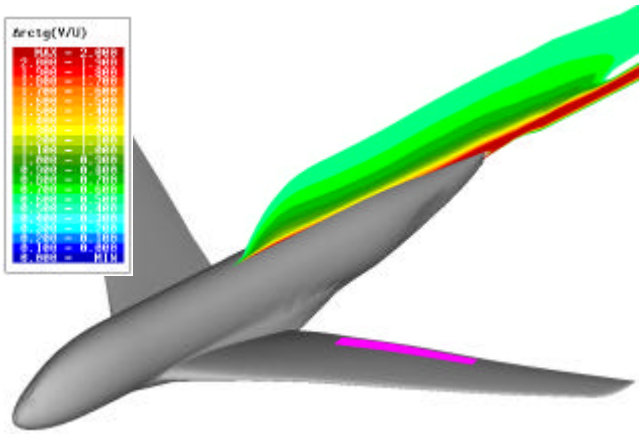

Figure 21 : b **field visualization on the fin area due to a** δs**=20° deflected spoiler on left wing**

In light of these numerical results, a conclusion is that the use of a complete mock up seems to be necessary for the correct assessment of rolling moment in wind tunnel test.

4 SUMMARY AND CONCLUSIONS

Two numerical applications have been carried out with ***elsA*** solver in order to study wing control devices effectiveness. Throughout their results, the non-coincident structured grid approach has proved its efficiency and should be integrated in the future Aero-Data generation process.

In the first application, aileron deflections are studied, using the Patched Grid technique coupled to a mesh deformation package, RAiD. Aileron deflection of a rigid wing has been simulated at first, showing an over-estimation of aileron effectiveness explained by an aero-elastic effects induced by aileron deflection. Even if bending and twist effect have been taken from HiReTT outcomes, this aero-elastic effect will be estimated by ***elsA*** solver as soon as the flexible matrix is built.

The second application uses a Chimera approach and deals with spoiler deployment. It permits to adequately estimate the spoilers' hinge moments and effectiveness (in terms of lift, drag and rolling moment), while keeping a simple mesh. Thanks to the Chimera method flexibility, a complete dissymmetrical aircraft mesh has been carried out, and an interaction right wing/left wing has been pointed out. These promising results should be improved in a near future, with the integration by ONERA into ***elsA*** solver of a multi-grid convergence acceleration technique compatible with the Chimera method [21].

In the prospect of speeding up even more the wing control surface meshing process, an automatic procedure based on HEXA© mesher, is thus in development in Airbus. Its goal will be to extract the spoiler geometry from the clean wing, to deploy it and, then, to generate the spoiler domain around.

ACKNOWLEDGEMENTS

The authors acknowledge the Airbus Methods and Tools team for their technical support, and especially Luis Barrera who follows all the study with a great attention.

CONTACTS

- guillaume.fillola@airbus.com
- Marie-Claire.Le_Pape@onera.fr
- Marc.Montagnac@cerfacs.fr

REFERENCES

[1] L. Cambier and M. Gazaix. "**elsA**: An Efficient Object-Oriented Solution to CFD Complexity", AIAA 2002-0108, *40th AIAA Aerospace Sciences Meeting and Exhibit*, Reno, 2002

[2] L.Barrera, Ch.Benoit, M.C. Le Pape, R.Houdeville, J.Peter, J.C. Jouhaud. "Advanced numerical simulations on structured grids for transport aircraft, using an efficient object oriented solver", *ICAS*, Toronto 2002 congress

[3] E. Goncalves, R. Houdeville. "Reassessment of the Wall functions Approach for RANS Computations", *Aerospace Science and Technologie*, Vol. 5, 2001, pp.1-14

[4] J.A. Benek, J.L. Steger and F.C. Dougherty. "A flexible embedding technique with application to the Euler equations". *AIAA* Paper 83-1944.

[5] P.M. Cali and V. Couaillier. "Conservative Interfacing for Overset Grids". *AIAA* Paper 2000-1008.

[6] M.M. Rai. "A Relaxation Approach to Patched-Grid Calculations with the Euler Equations". *Journal of Computational Physics 66*, 99-131, 1986.

[7] R.W. Walters and J.L. Thomas. "A Patched-Grid Algorithm for Complex Aircraft Configurations". *Proceedings of the third international symposium on domain decomposition methods for partial differential equations* pp397-416, SIAM, 1990.

[8] A. Lerat and Z.N. Wu. "Stable Conservative Multidomain Treatments for Implicit Euler Solvers". *Journal of Computational Physics* 123, 45-64 (1996).

[9] H. Chen and S. Fu. "Navier-Stokes Simulations for Transport Aircraft Wing/Body High-Lift Configurations". *Journal of Aircraft*. Vol. 40, No. 5, September-October 2003.

[10] A. Benkenida, J. Bohbot and J. C. Jouhaud. "Patched grid and adaptive mesh refinement strategies for the calculation of the transport of vortices". *International Journal of Numerical Methods in Fluids*, 40(7):855-873, 2002.

[11] I. Sutherland and G. Hodgman. "Reentrant polygon clipping". *Communications of the ACM*, 17(1): 32-42, January 1974

[12] J.L. Steger, F.C Dougherty and J.A. Benek. "A Chimera grid scheme", *ASME Mini symposium on advances in grid generation*, Houston (USA), June 1993.

[13] M.-C. Le Pape, D. Darracq and P. Guillen. "Design of a Chimera unsteady code, application to store separation" , *7th International symposiun on CFD*, Beijing (China), 1997.

[14] G. Jeanfaivre., Ch. Benoit and M.-C. Le Pape. "Improvement of the robustness of the Chimera method", *AIAA Fluid Dynamics Conference and Exhibit, St-Louis (USA)*, June 2002.

[15] R.Collercandy. "HiReTT, the application of CFD to resolve the flow in the ETW test section", *Katnet/Garteur Second Workshop*, Bath, September 2003

[16] Ralf Mertins, Birol Colak, Samira Barakat and Eberhard Elsholz. "3D viscous flow analysis on wing-body-aileron-spoiler configurations" *DGLR congress*, Munich, November 2003.

[17] M.Meaux, M.Cormery and G.Voizard. "Viscous aerodynamic shape optimization based on the discrete adjoint state for 3D industrial configuration", *ECCOMAS*, 2004

[18] F. Jiang. "CFD Modeling of 2-D Aileron effectiveness". SAE 1999, *World Aviation Conference*. San Francisco, 1999-01-5618 October 1999.

[19] C.Braun, A.Boucke, G.Wellmer, A.Karavas and J.Ballmann. "Numerical Prediction of the Influence of Deployed Aileron and Dynamic Pressure on the Model Deformation of a High Speed Transport Aircraft Type Wing by Direct Aeroelastic Simulation". *HiReTT project*, August 2003

[20] Schwarz, T.: "Development of a wall treatment for Navier-Stokes Computations using the Overset-Grid Technique", *26th European Rotorcraft Forum*, The Hague, The Netherlands, September 2000

[21] X.Juvigny, E. Canonne and C.Benoit. "Multigrid Algorithms for the Chimera method", *42th AIAA Aerospace Sciences Meeting & Exhibit*, January 2004